doi:10.1246/cl.2013.310
Published on the web March 2, 2013

Temperature-dependent Upconversion Luminescence of $NaYF_4$:Yb^{3+},Er^{3+} Nanoparticles

Junwei Zhao,*[1] Haitao Li,[1] Qinghui Zeng,[2] Kai Song,[3] Xiaofeng Wang,[1] and Xianggui Kong*[2]
[1]*Department of Materials Science and Engineering, Luoyang Institute of Science and Technology, Luoyang 471023, P. R. China*
[2]*State Key Laboratory of Luminescence and Applications, Changchun Institute of Optics, Fine Mechanics and Physics, Chinese Academy of Sciences, Changchun 130033, P. R. China*
[3]*School of Life Sciences, Changchun Normal University, Changchun 130032, P. R. China*

(Received November 26, 2012; CL-121178)

The temperature-dependent quenching characteristics of the upconversion luminescence in $NaYF_4$:Yb^{3+},Er^{3+} nanoparticles under 980-nm excitation are reported. Intense green and red upconversion emissions corresponding to the ($^2H_{11/2}$, $^4S_{3/2}$) → $^4I_{15/2}$ and $^4F_{9/2}$ → $^4I_{15/2}$ transitions of the Er^{3+} ions were observed. The green emission at around 520 nm presents a continuous increase with increasing temperature, while the emission bands at around 545 and 657 nm decrease with the temperature change from 84 to 364 K. The temperature dependence of the intensity characteristics was analyzed systematically by using a simple three-level system.

Upconversion luminescence is considered as a promising solution for obtaining efficient biological labeling, imaging, and therapy.[1] Over the past decade, the upconversion luminescence of lanthanide-doped nanomaterials has become more prominent in the biological sciences owing to their unique energy-level structures and luminescent properties.[2–7] It is important for lanthanide ions to choose appropriate host materials for high-efficiency upconversion signals to be obtained.[8] In recent years, fluoride matrixes have received more attention owing to their relatively low phonon energy.[9,10] Their low maximum phonon energy leads to low nonradiative decay rates and high radiative emission rates for the energy levels of lanthanide ions.[9,10] Therefore, strong upconversion emission can be observed easily in Er-doped fluoride nanoparticles at room temperature, and the upconversion mechanisms have been analyzed in detail. It is well known that $NaYF_4$ has been regarded as the most effective host material for upconversion luminescence.[3,10] Most reports on $NaYF_4$ nanoparticles focus on their synthesis, upconversion luminescence at room temperature, and biomedical experiments as proofs of concept.[1,2,11] However, to the best of our knowledge, there has been no report on the temperature dependence of upconversion luminescence processes involving Er ions doped into $NaYF_4$ nanoparticles. The development of cryogenic temperature equipment has provided the technology for studying the optical properties of materials.[12–16] In this paper, the temperature quenching characteristics of the infrared-to-visible upconversion luminescence of $NaYF_4$:Yb^{3+},Er^{3+} nanoparticles are reported, and the dependence of the intensity characteristics on the temperature is analyzed systematically by a simple three-level system.

The $NaYF_4$: 10 mol % Yb^{3+}, 1 mol % Er^{3+} nanoparticles were synthesized as described in our previous reports.[17,18] The upconversion emission spectra of Er^{3+} in the $NaYF_4$ nanoparticles were acquired using a Jobin–Yvon LabRam Raman spectrometer system equipped with a Peltier air-cooled CCD detector and holographic gratings with 1800 and 600 grooves/mm. Precise control of the sample temperature (0.1 °C) was achieved by means of a Linkam THMS600 temperature-programmable heating/cooling microscope stage. The THMS stage was used in conjunction with a Linkam LNP cooling system when cooling. Samples were excited by a semiconductor diode laser with a wavelength of 980 nm.

Figure 1 shows the XRD pattern and SEM image of the $NaYF_4$:Yb^{3+},Er^{3+} nanoparticles. As seen from Figure 1a, the

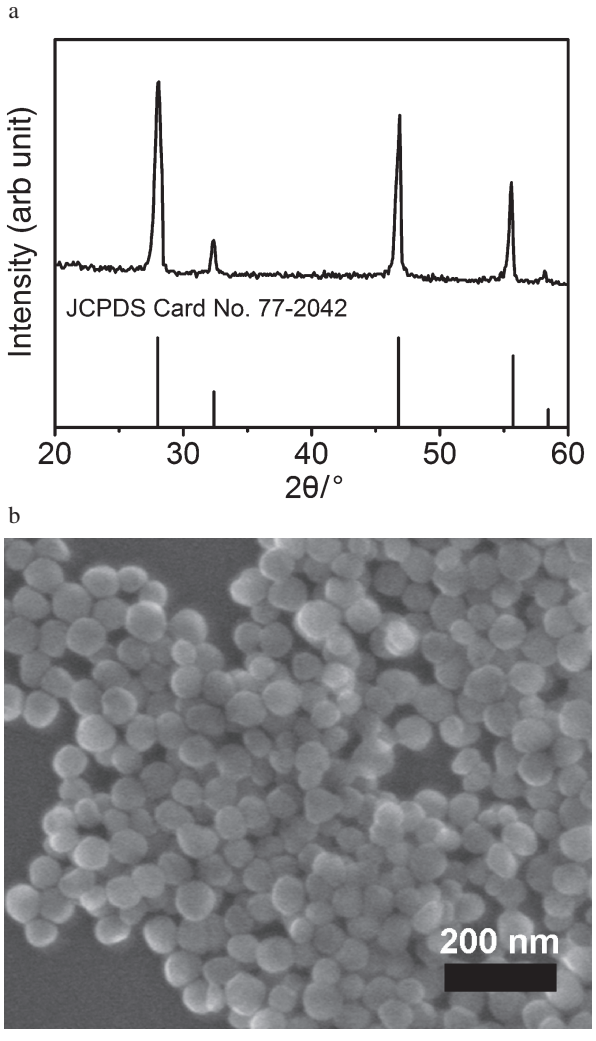

Figure 1. XRD pattern (a) and SEM image (b) of $NaYF_4$:Yb^{3+},Er^{3+} nanoparticles.

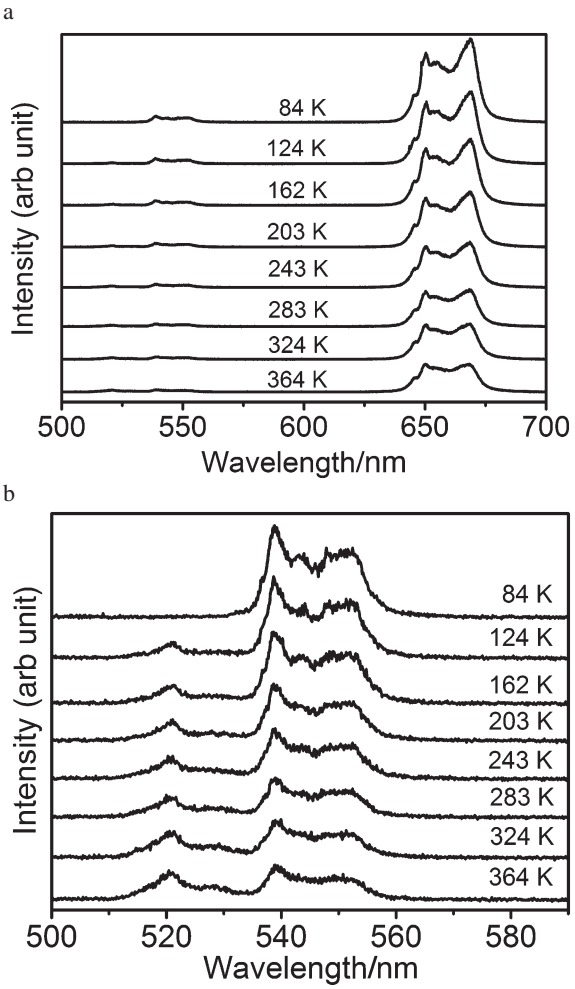

Figure 2. Upconversion luminescence spectra of $NaYF_4$: 10 mol % Yb^{3+}, 1 mol % Er^{3+} nanoparticles excited by CW laser radiation at 980 nm at different temperatures.

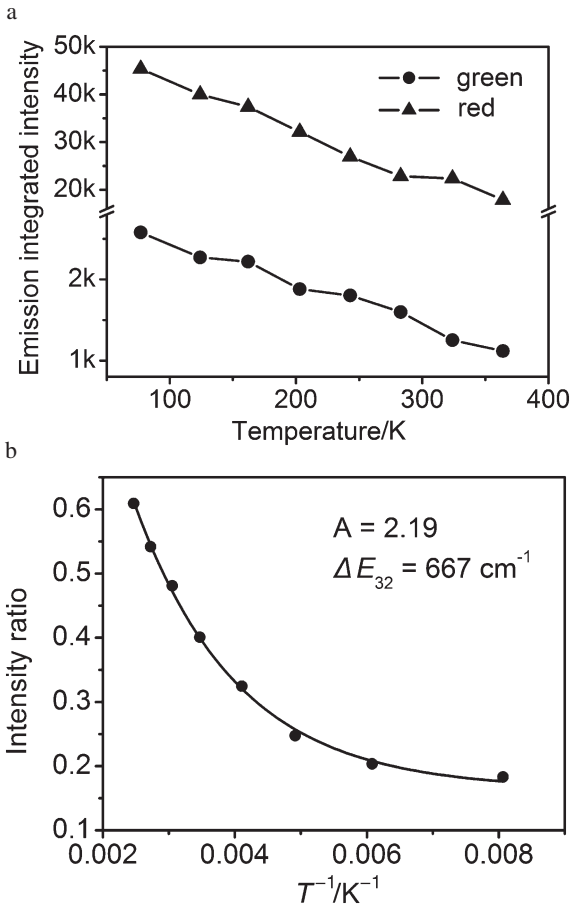

Figure 3. (a) Green and red upconversion emission intensity as a function of temperature and (b) the integrated intensity ratio of the $^2H_{11/2} \rightarrow {}^4I_{15/2}$ to $^4S_{3/2} \rightarrow {}^4I_{15/2}$ transitions as a function of the absolute temperature ($1/T$).

XRD peaks match well with those of standard cubic-phase $NaYF_4$ (PDF Card No. 77-2042). The peaks shown in the XRD pattern are sharp and intense, indicating good crystallization of the sample.[17,18] It is observed that the obtained $NaYF_4$:Yb^{3+},Er^{3+} nanoparticles are spherical and monodisperse with an average diameter of about 40 nm (Figure 1b).

Figure 2a shows the upconversion luminescence spectra of $NaYF_4$: 10 mol % Yb^{3+}, 1 mol % Er^{3+} nanoparticles excited by CW laser radiation (980 nm) at different temperatures. Figure 2b shows the magnification of the green emission at different temperatures. The green emission bands were observed at 520 and 545 nm, corresponding to the $^2H_{11/2} \rightarrow {}^4I_{15/2}$ and $^4S_{3/2} \rightarrow {}^4I_{15/2}$ transitions of the Er^{3+} ions. The red emission bands were observed at 657 nm, corresponding to the $^4F_{9/2} \rightarrow {}^4I_{15/2}$ transitions of the Er^{3+} ions. It is worth noting that the three upconversion emission bands change greatly with the temperature. Interestingly, the upconversion luminescence at 520 nm cannot be detected clearly when the temperature is below 124 K. At 84 K, the transition from the $^2H_{11/2}$ level to the ground state was not observed, while both the emissions of the $^4S_{3/2} \rightarrow {}^4I_{15/2}$ and $^4F_{9/2} \rightarrow {}^4I_{15/2}$ transitions could be observed clearly. However, as the temperature was increased to 124 K, the $^2H_{11/2} \rightarrow {}^4I_{15/2}$ transition was just observed, which is the well-known green hot band (Figure 2b). Following the measuring temperature increase from 124 to 364 K, the upconversion luminescence intensity of the $^2H_{11/2} \rightarrow {}^4I_{15/2}$ transition increased all the time; on the contrary, the $^4S_{3/2} \rightarrow {}^4I_{15/2}$ transition decreased. As we know, the $^2H_{11/2}$ population occurs at the expense of the $^4S_{3/2}$ depopulation because the $^4S_{3/2}$ state is the feeding level for the $^2H_{11/2}$ level.[13–15] More $^2H_{11/2}$ Stark levels are populated by the electrons produced by thermal excitation with the increase in temperature. The macroscopic effect is the broadening of the 520-nm emission band with increasing temperature (Figure 2b). Meanwhile, the total intensities of the green and red emissions corresponding to the $^4S_{3/2} \rightarrow {}^4I_{15/2}$ and $^4F_{9/2} \rightarrow {}^4I_{15/2}$ transitions both decreased nonlinearly with increasing temperature (Figure 3a).

Finally, the relative populations of the $^4S_{3/2}$ and $^2H_{11/2}$ levels can be predicted using a three-level model, which is composed of the $^4I_{15/2}$ ground level (level 1), the $^4S_{3/2}$ excited level (level 2), and the $^2H_{11/2}$ excited level (level 3). The following equation can be used to express the thermalization of the $^2H_{11/2}$ level:[12–15]

$$\frac{I_3}{I_2} = A \exp\left(\frac{-\Delta E_{32}}{kT}\right) \quad (1)$$

where I_3 and I_2 are the integrated upconversion emission intensities of the $^2H_{11/2} \rightarrow {}^4I_{15/2}$ and $^4S_{3/2} \rightarrow {}^4I_{15/2}$ transitions of the Er^{3+} ion, respectively, T is the absolute temperature, k is Boltzmann's constant, and ΔE_{32} is the energy gap between the $^2H_{11/2}$ and $^4S_{3/2}$ levels. The pre-exponential factor, A, is expressed by the following equation:[12,14,15]

$$A = \frac{W_{R3} g_3 h\nu_3}{W_{R2} g_2 h\nu_2} \quad (2)$$

where W_{R3} and W_{R2} are the radiative probabilities of the two transitions, $h\nu_3$ and $h\nu_2$ are the photon energies of the respective transitions from levels 3 and 2 to level 1, and g_3 and g_2 are the $(2J + 1)$ degeneracies of levels 3 and 2, respectively. The calculated values of I_3/I_2 as a function of $1/T$ were fitted using a single exponential function; from this function, an energy gap of 667 cm^{-1} was obtained (Figure 3b). This value is consistent with the estimated energy difference ($\Delta E_{32} = 690\,cm^{-1}$) between the lowest-energy $^4S_{3/2}$ Stark level and the highest-energy $^2H_{11/2}$ Stark level from the upconversion luminescence spectra. The A parameter is 2.19, indicating that the radiative transition probability W_{R3} is greater than W_{R2}.

In summary, the temperature quenching characteristics of the infrared-to-visible upconversion emission in $NaYF_4:Yb^{3+},Er^{3+}$ nanoparticles excited at 980 nm at cryogenic temperatures have been reported. The green emission at around 520 nm shows a continuous increase with increasing temperature. The green emission at around 545 nm and the red emission at around 657 nm decrease as the temperature changes from 84 to 364 K. The dependence of the intensity characteristics on temperature was analyzed systematically by using a simple three-level system. The results presented in this study may provide new insights for the further development of upconversion luminescence in nanoparticles.

This work was supported financially by the National Natural Science Foundation of China (Grant Nos. 11204122, 61275197, and 11204021), and the Natural Science Research Project of the Education Department of Henan Province (Grant No. 12B430016).

References

1 F. Wang, D. Banerjee, Y. Liu, X. Chen, X. Liu, *Analyst* **2010**, *135*, 1839.
2 F. Wang, X. Liu, *Chem. Soc. Rev.* **2009**, *38*, 976.
3 F. Auzel, *Chem. Rev.* **2004**, *104*, 139.
4 J. Zhou, X. Zhu, M. Chen, Y. Sun, F. Li, *Biomaterials* **2012**, *33*, 6201.
5 A. Xia, M. Chen, Y. Gao, D. Wu, W. Feng, F. Li, *Biomaterials* **2012**, *33*, 5394.
6 L.-L. Li, R. Zhang, L. Yin, K. Zheng, W. Qin, P. R. Selvin, Y. Lu, *Angew. Chem., Int. Ed.* **2012**, *51*, 6121.
7 A. Zhou, Y. Wei, B. Wu, Q. Chen, D. Xing, *Mol. Pharmaceutics* **2012**, *9*, 1580.
8 J. Shen, L.-D. Sun, C.-H. Yan, *Dalton Trans.* **2008**, 5687.
9 P. Rahman, M. Green, *Nanoscale* **2009**, *1*, 214.
10 C. Li, J. Lin, *J. Mater. Chem.* **2010**, *20*, 6831.
11 N. M. Idris, M. K. Gnanasammandhan, J. Zhang, P. C. Ho, R. Mahendran, Y. Zhang, *Nat. Med.* **2012**, *18*, 1580.
12 W. Xu, S. Dai, L. M. Toth, G. D. Del Cui, J. R. Peterson, *J. Phys. Chem.* **1995**, *99*, 4447.
13 F. Vetrone, J. C. Boyer, J. A. Capobianco, A. Speghini, M. Bettinelli, *J. Phys. Chem. B* **2002**, *106*, 5622.
14 X. Wang, X. Kong, G. Shan, Y. Yu, Y. Sun, L. Feng, K. Chao, S. Lu, Y. Li, *J. Phys. Chem. B* **2004**, *108*, 18408.
15 Y. Sun, H. Liu, X. Wang, X. Kong, H. Zhang, *Chem. Mater.* **2006**, *18*, 2726.
16 X. Shen, Q. Nie, T. Xu, S. Dai, X. Wang, *J. Lumin.* **2010**, *130*, 1353.
17 Y. Sun, Y. Chen, L. Tian, Y. Yu, X. Kong, J. Zhao, H. Zhang, *Nanotechnology* **2007**, *18*, 275609.
18 J. Zhao, Y. Sun, X. Kong, L. Tian, Y. Wang, L. Tu, J. Zhao, H. Zhang, *J. Phys. Chem. B* **2008**, *112*, 15666.

